

Shear Load Transfer Characteristics of Drilled Shafts Socketed in Rocks

Sangseom Jeong · Sangyong Ahn · Hoonil Seol

Received: 19 December 2007 / Accepted: 12 December 2008 / Published online: 3 February 2009
© Springer-Verlag 2009

Abstract This paper presents a shear load transfer function and an analytical method for estimating the load transfer characteristics of rock-socketed drilled shafts subjected to axial loads. A shear load transfer ($f-w$) function of rock-socketed drilled shafts is proposed based on the constant normal stiffness (CNS) direct shear tests. It is presented in terms of the borehole roughness and the geological strength index (GSI) so that the structural discontinuities and the surface conditions of the rock mass can be considered. An analytical method that takes into account the coupled soil resistance effects is proposed using a modified Mindlin's point load solution. Through comparisons with load test results, the proposed methodology is in good agreement with the general trend observed in in situ measurements and represents an improvement in the prediction of the shear behavior of rock-socketed drilled shafts.

Keywords Rock-socketed drilled shaft · Load transfer function · Constant normal stiffness direct shear test · Borehole roughness · Coupled soil resistance · Pile-rock interface

1 Introduction

In South Korea, a number of large construction projects, such as land reclamation for an international airport, high-

speed railways, and harbor construction, are in progress in urban and coastal areas. Drilled shafts are frequently used in those areas as a viable replacement for driven piles for two applications: deepwater offshore foundations and foundations in urban areas where noise and vibration are not tolerated. Over 90% of the drilled shafts constructed in South Korea are embedded in weathered or soft rocks.

Rock-socketed drilled shafts typically carry most of their working load in shaft resistance because the ultimate shaft resistance is generally mobilized at smaller interface displacements between the shaft and surrounding rock than the ultimate toe resistance. Williams et al. (1980) and Carter and Kulhawy (1988) reported that the typical range of load transmitted to the pile toe, expressed as a percentage of the axial load applied at the pile head, is 10–20% at typical working loads.

The load transfer method is widely used to predict the load transfer characteristics of piles subjected to an axial load because it has a simple analytical procedure and can be applied to any soil profile, which may be complex, and be a pile with a diameter that varies with depth. In this method, load transfer functions describe the relationship between the unit resistance transferred to the surrounding soil and the displacement of the pile relative to each soil layer. A few shear load transfer ($f-w$ or $t-z$) functions have been proposed to analyze the load transfer of a pile socketed in rocks (Baguelin 1982; O'Neill and Hassan 1994).

O'Neill and Hassan (1994) suggested potential $f-w$ behavior in rock, as shown in Fig. 1. If the pile-rock interface is clean, the cement paste bonds to the rock, the roughness pattern is regular, and the asperities are rigid, an $f-w$ relation such as OABC can be obtained. In most cases, however, the interface asperity pattern is not regular. In addition, asperities are deformable, which results in ductile, progressive failure among asperities. Therefore, O'Neill

S. Jeong (✉) · H. Seol
Department of Civil Engineering, Yonsei University,
Seoul 120-749, Korea
e-mail: soj9081@yonsei.ac.kr

S. Ahn
Department of Railway and Mass Transit,
Daewoo Engineering, Seongnam 463-825, Korea

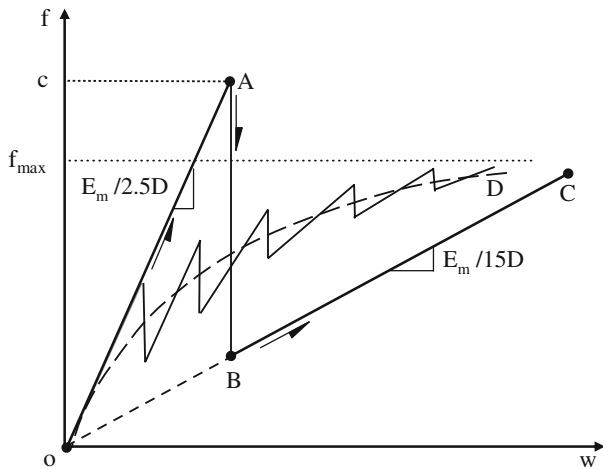


Fig. 1 Potential f - w relations for rock (O'Neill and Hassan 1994)

and Hassan (1994) proposed a hyperbolic f - w model that describes shear load transfer behavior for most rock types, as shown in Fig. 1 and Eq. 1:

$$f = \frac{w}{\frac{2.5D}{E_m} + \frac{w}{f_{\max}}} \quad (1)$$

where w is the pile displacement, f_{\max} is the maximum unit shaft resistance, D is the pile diameter, and E_m is the effective Young's modulus of the rock mass.

However, these f - w models are only reliable if site-specific correlations are developed. Even so, their reliability may be questionable, because they exclude many variables that affect the shaft resistance of rock sockets (Johnston 1994; Kim et al. 1999; Seol 2007).

The important role of soil-pile interaction in the analysis and design of foundations has long been recognized by geotechnical engineers. The load transfer method models the pile as a series of discrete elements, and the relationship between pile displacement and soil resistance is represented by independent springs. As a result, the continuity of soil mass is not properly taken into account, and, hence, the coupled soil resistance, in which the response at any point on the interface affects other points, is neglected.

This paper is intended to evaluate the load transfer characteristics of drilled shafts installed in rocks. The f - w function is proposed to take into account various factors that influence the shaft resistance mechanism, such as pile and rock properties, pile-soil interface geometry and slip characteristics, and the type and amount of rock weathering. The validity of this study was tested through field case studies.

2 Constant Normal Stiffness Direct Shear Test

Artificially made pile-rock interfaces with a series of regular sawtooth asperities were tested to analyze the basic

mechanism and the effect of influential factors such as roughness, normal stiffness, initial normal stress, and unconfined compressive strength (UCS). The mechanisms established from constant normal stiffness (CNS) direct shear tests were applied to predict the performance of the shear load transfer of rock-socketed drilled shafts.

2.1 Quantification of Borehole Roughness

Before performing a CNS test, a quantitative analysis of borehole roughness should be carried out to determine the objective roughness represented as a natural irregular profile of the borehole surface. Seidel and Haberfield (1995) recommended that roughness be scale-dependent and, therefore, all roughness statistics must be accompanied by a measure of scale in order for them to be meaningful. This method is based on an idealized joint interface that is modeled as a series of interconnected chords with a constant length (l_a), as shown in Fig. 2. It is assumed that the chord angle (θ) is normally distributed with mean (μ_θ) and standard deviation (s_θ). Thus, the asperity heights (Δr) will vary in the distribution, which can be approximated as Gaussian for reasonable socket roughness and can be represented as follows:

$$\Delta r = \frac{1}{n} \sum_{i=1}^n |\Delta r_i| = \frac{1}{n} \sum_{i=1}^n |l_a \sin |\bar{\theta}|| \quad (2)$$

Based on this approach, the natural irregular profile of a borehole can be simplified to a regular sawtooth pattern. It is critical to note that Δr depends on l_a , and, thus, l_a should be determined on the basis of the converged value of Δr .

The quantified values of roughness determined in previous studies and this study are summarized in Table 1. Seidel and Collingwood (2001) present bounds of roughness height as a function of the UCS of intact rock based on back-analysis of the existing load tests. Nam (2004) evaluated the borehole roughness, which is constructed separately with an auger and core barrel, of four sites in clayshale and limestone using a chord length l_a of 50 mm. Lee et al. (2003) measured the borehole roughness of granite, gneiss, sandstone, and andesite at ten different sites (15 boreholes) in Korean peninsula. They report that the representative chord length of borehole roughness in gneiss-granite is approximately 50 mm and the roughness height Δr ranges from 1 to 5.1 mm, regardless of the rock type. These ranges include the measured roughness heights

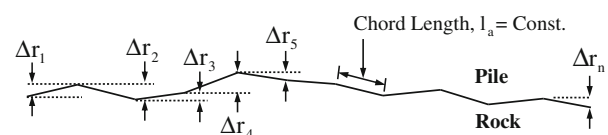


Fig. 2 Monash socket roughness model (Seidel and Haberfield 1995)

Table 1 Quantified values of roughness for rock socket ($l_a = 50$ mm)

	Rock type	UCS (MPa)	Roughness height (mm)	Roughness angle ($^\circ$)	Remark
This study	Gneiss	5–50	1–7	1.1–8.0	Bit
Seidel and Collingwood (2001)	Claystone, sandstone, shale, limestone, etc.	5–10 10–70	1.7–16.2 0.9–6.6	1.9–18.9 1.0–7.6	Back-analysis
Lee et al. (2003)	Granite	100–150	1–5.1	1.1–5.9	RCD/all casing
	Gneiss	30–130	1–4	1.1–4.6	
	Sandstone	75–77			
Nam (2004)	Andesite	74	1–3.5	1.1–4.0	
	Clayshale	1–4	3.6–5.3	4.1–6.1	Auger
			4.7–5.8	5.4–6.7	Core barrel
	Limestone	10	3.2–3.7 4.3–5.1	3.7–4.2 4.9–5.8	Auger Core barrel

(1–7 mm) of two test sites in this study. Based on the results, the borehole roughness of a rock socket can be represented by a regular sawtooth roughness with a chord length l_a of 50 mm and roughness heights Δr from 1 to 16.2 mm, which correspond to roughness angles i that range from 1.1 to 18.9°.

2.2 Sample Preparation and Testing Apparatus

Natural rock blocks with quantified sawtooth roughness are required for CNS tests. It is impossible to perform a large number of CNS tests under various boundary conditions because it is difficult to prepare large rock block samples and to make regular asperity patterns with rock blocks that include discontinuities. Therefore, two industrial gypsum plasters were used to make an idealized sawtooth rock sample. They can be molded into any shape when mixed with water, and the long-term strength is independent of time once the chemical hydration is complete. To prepare the pile sample, cement mortar, which consists of cement and sand, was substituted for concrete because concrete contains large aggregates which can be difficult to fit into laboratory-scale test samples. The property values of plaster are typical of most sedimentary rocks (Indraratna et al. 1998). Table 2 summarizes the UCS and the Young’s modulus (E_s) of the two cured plasters and cement mortar that are used in this study.

Table 2 Material properties of constant normal stiffness (CNS) direct shear test samples

Parameters	Artificial rock A	Artificial rock B	Drilled shaft
Material type	Gypsum plaster	Gypsum plaster	Cement mortar
UCS (MPa)	20	35	42
E_s (MPa)	2,720	3,550	–

Referring to the quantified borehole roughness, test samples are molded by gypsum plaster and cement mortar with asperity angles of 4.6, 9.1, and 15.6° and a chord length of 25 mm, as shown in Fig. 3.

To model pile–rock interfaces properly in the laboratory, a CNS direct shear testing apparatus provides large-size samples with varying shear area, an exact measurement of the vertical and horizontal displacement, and accurate loading according to displacements. The main part of the CNS testing apparatus used in this study comprises normal and shear sections with servo-controlled hydraulic actuators, load cells, and LVDT transducers. The split shear boxes holding the matching half-samples of rock and concrete have maximum internal dimensions of 150 × 200 × 100 mm high.

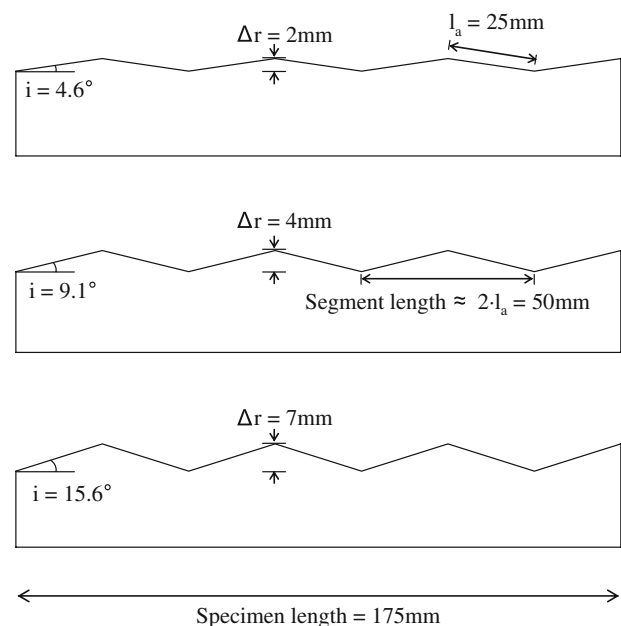


Fig. 3 Sawtooth specimen for CNS direct shear test (gypsum plaster)

2.3 Test Conditions and Procedure

To study the influential factors of shaft resistance of rock-socketed drilled shafts, the CNS direct shear tests were conducted on sawtooth samples under various normal stiffnesses and initial normal stresses. A summary of the test boundary conditions is given in Table 3. The normal stiffness K_n of a rock-socketed drilled shaft can be determined conventionally using the theoretical analysis of an expanding infinite cylindrical cavity in an elastic half-space (Boresi 1965) as follows:

$$K_n = \frac{\Delta\sigma_n}{\Delta r} = \frac{E_m}{r(1 + \nu_m)} \quad (3)$$

where $\Delta\sigma_n$ is the increased normal stress, Δr is the dilation, r is the radius of a pile, and E_m and ν_m are the deformation modulus and Poisson's ratio of the rock mass, respectively. The normal stiffness used in this study varied from 0.2 to 1.0 MPa/mm based on back-calculation using the general properties of the rock-socketed pile.

The initial normal stress (σ_{n0}) is imposed on the side wall of a rock socket by a head of wet concrete and depends on complex influential factors, such as the cast velocity of concrete, the arching effect of aggregates, the hardening rate, the degree of compaction, and the shrinkage rate of cement (Taylor 1965). Since it is difficult to conveniently incorporate all of these factors, the initial normal stress can simply be assumed to be a function of the cast depth of the concrete based on the theory of fluid static mechanics.

2.4 Test Results and Discussion

A total of 54 individual tests were conducted under the various boundary conditions described in the previous sections (Table 3). Based on the results of the CNS tests, the shear behavior of regular sawtooth rock joints under CNS conditions could be classified as: (1) elastic (SP1), a non-slipping or sticking state in which normal stress is constant due to no dilation before a slip at the joint interface; (2) elasto-plastic (SP2), the slipping state in which dilation of the joint interface occurs during shearing and causes an additional normal stress and shear stress; (3) plastic (SP3), the residual state in which the normal and shear stress are maintained or reduced due to rupture of the

asperities. In this paper, only some typical CNS test results are presented.

Figure 4 shows the results from three typical tests on artificial rock sample A with different roughness angles (4.6, 9.1, and 15.6°) under the conditions of 0.5 MPa/mm normal stiffness and 0.35 MPa initial normal stress. More specifically, the following quantities are plotted: shear stress–shear displacement (τ – w), normal displacement–shear displacement (ψ – w), shear stress–normal stress (τ – σ_n), and normal displacement–normal stress (ψ – σ_n). As the roughness angle i increases, the amount of normal displacement increases in the elasto-plastic portion (SP2), as shown in the normal displacement–shear displacement (ψ – w) curves of Fig. 4a, thus, the normal stress increases

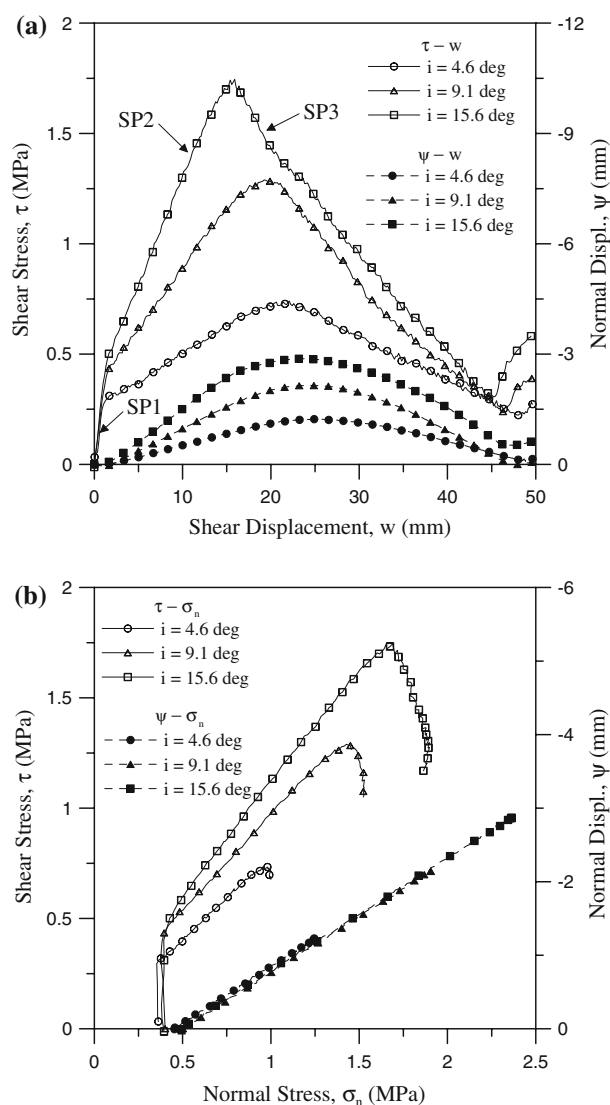


Fig. 4 Effect of roughness height (rock specimen A, under normal stiffness 0.5 MPa/mm, initial stress 0.35 MPa): **a** shear stress and normal displacement with shear displacement, **b** shear stress and normal displacement with normal stress

Table 3 Summary of the test boundary conditions

Variable	Values
Roughness angle, i (°)	4.6, 9.1, 15.6
Normal stiffness, K_n (MPa/mm)	0.2, 0.5, 1.0
Initial normal stress, σ_{n0} (MPa)	0.35, 0.70, 1.05

as illustrated in the normal displacement–normal stress ($\psi-\sigma_n$) curves of Fig. 4b. Consequently, the increased normal stress induces increased shear stress proportionately, as shown in the shear stress–normal stress ($\tau-\sigma_n$) curves of Fig. 4b.

These results are similar to those for a roughness angle of 9.1° under the same initial normal stress (0.35 MPa) with three normal stiffnesses (0.2, 0.5, and 1.0 MPa/mm), as shown in Fig. 5. The peak shear stress tends to increase as the normal stiffness increases. This is explained by the fact that the normal stress tends to be increased by an increase in normal stiffness, even if both samples have the same roughness. However, while the slopes of shear stress versus normal stress curves are the same regardless of

normal stiffness, they differ slightly with different roughness angles.

Figure 6 shows the shear responses under the condition of 0.5 MPa/mm normal stiffness and three different initial normal stresses (0.35, 0.70, and 1.05 MPa) with a roughness angle of 4.6° . The results demonstrate that the peak shear stress tends to increase with the initial normal stress as well as the roughness angle, and normal stiffness also increases. However, the initial normal stress has an effect on the shear stiffness and strength of SP1 only before slipping occurs. In addition, the initial peak strengths of CNS tests are smaller than those of a natural rock-socketed pile because the samples of rock and concrete are molded separately, so no bonding exists between them. Once

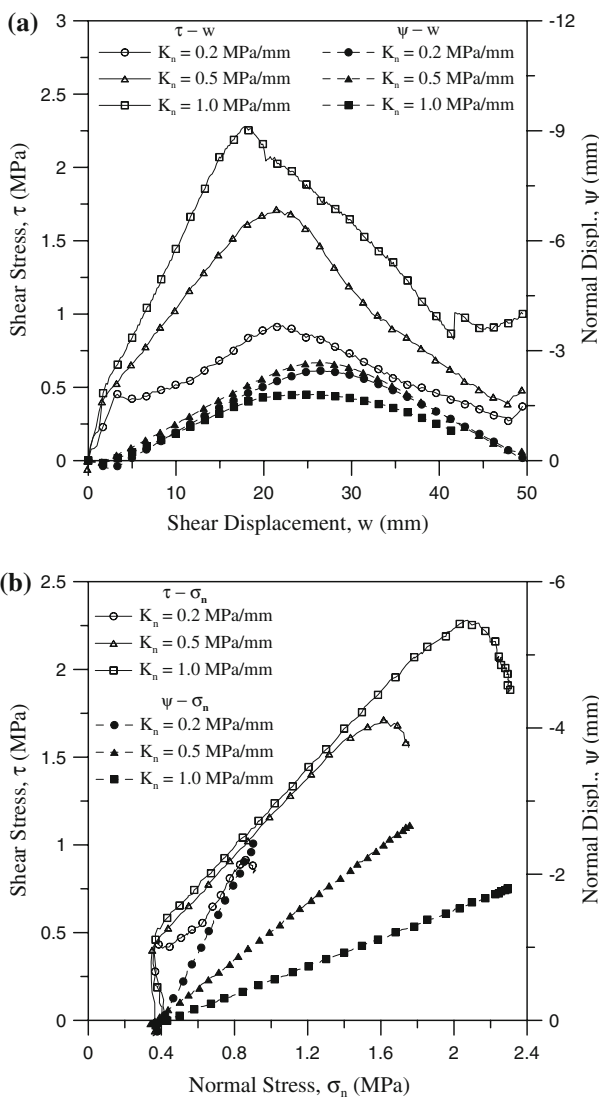


Fig. 5 Effect of normal stiffness (rock specimen B, under roughness height 4 mm, initial stress 0.35 MPa): **a** shear stress and normal displacement with shear displacement, **b** shear stress and normal displacement with normal stress

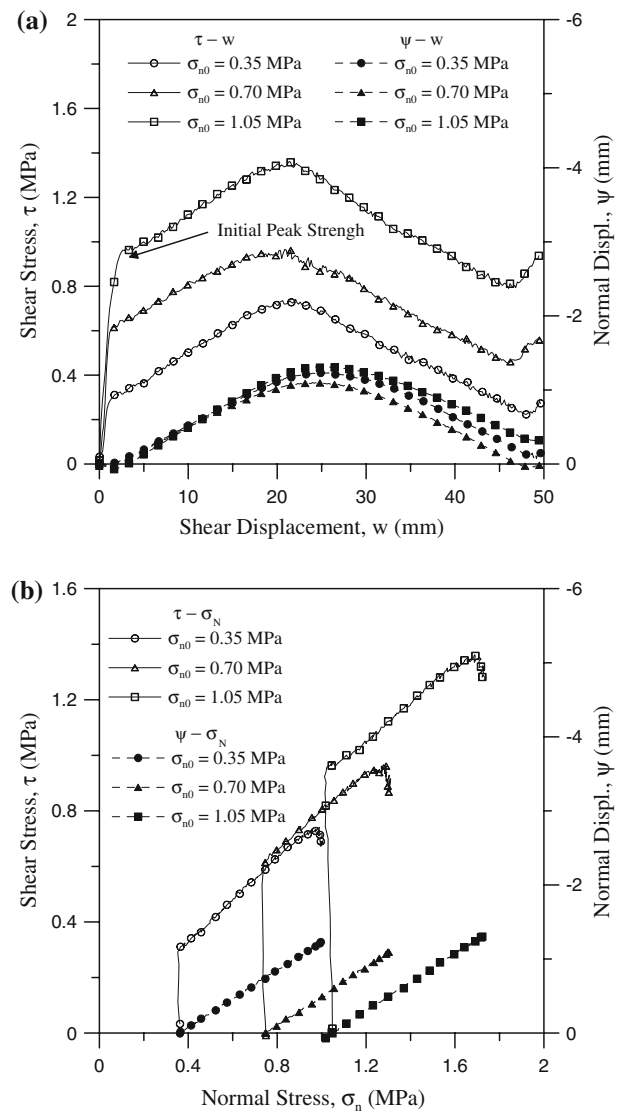


Fig. 6 Effect of initial stress (rock specimen A, under roughness height 2 mm, normal stiffness 0.5 MPa/mm): **a** shear stress and normal displacement with shear displacement, **b** shear stress and normal displacement with normal stress

slippage occurs, however, cohesion at the interface disappears so that the bonding effects may be ignored.

3 Proposed Shear Load Transfer Function

Based on the CNS tests, the shear stiffness of the elastic portion (SP1) depends on the initial normal stress, while that of the elasto-plastic portion (SP2) depends on both rock socket roughness and normal stiffness. It has also been known that a reduction in joint shear strength is influenced by the rock mass characteristics, such as rock type, joint structure, and weathering of the joint wall. To consider the various factors of shear behavior at the pile–rock interface, a new method for the shear load transfer function of rock-socketed drilled shafts is proposed based on the Hoek–Brown failure criterion.

The mechanical behavior of a pile–rock interface is a specific case of the mechanical behavior of all problems involving rock–rock joints. A significant amount of research on the shear behavior of pile–rock interfaces has been carried out extensively and diversely from the research of rock–rock joints (Ooi 1989; Seidel and Haberfield 1995; Indraratna et al. 1998). The criterion of Hoek and Brown (1997), which is based on the assessment of interlocking rock blocks and the condition of the surfaces between these blocks, is defined as follows:

$$\sigma'_1 = \sigma'_3 + \sigma_{ci} \left(m_b \frac{\sigma'_3}{\sigma_{ci}} + s \right)^a \tag{4}$$

where σ'_1 and σ'_3 are the major and minor effective principal stresses at failure, respectively, σ_{ci} is the UCS of an intact rock, m_b is the reduced value of the material constant m_i for a rock mass, and s and a are the constants that depend on the rock mass characteristics. Equation 4, which is expressed in terms of the major and minor principal stresses, can be rewritten as a nonlinear relationship (see Fig. 7a) between shear and normal stresses as follows (Hoek and Brown 1997):

$$\tau = A\sigma_{ci} \left(\frac{\sigma'_n - \sigma_{tm}}{\sigma_{ci}} \right)^B \tag{5}$$

where τ is the shear strength for which the unit shaft resistance f can be substituted, A and B are regression constants, σ'_n is the effective normal stress, and σ_{tm} is the tensile strength of the rock mass, which is $s\sigma_{ci}/m_b$.

Once this envelope (Eq. 5) is transferred in relation to shear stress and shear displacement, the shear load transfer function of the rock-socketed pile can be expressed as a nonlinear triple curve, consisting of three parts as shown in Fig. 7b: a linear pre-slip portion (SP1), a nonlinear slip portion (SP2), and a post-slip portion (SP3).

The normal stress σ'_n can be obtained by summing up the initial normal stress σ_{n0} and increments of normal stress $\Delta\sigma_n$ as follows:

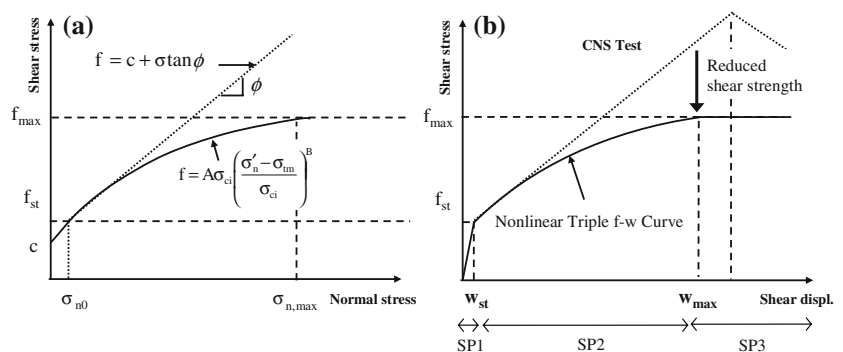
$$\sigma'_n = \sigma_{n0} + \Delta\sigma_n = \sigma_{n0} + K_n(w - w_{st}) \tan i \tag{6}$$

where σ_{n0} is a function of the cast depth z of the concrete based on the theory of static fluid mechanics and $\Delta\sigma_n$ is obtained from the product of the normal stiffness K_n and normal displacement ψ , which is calculated in turn from the relative displacement of the pile–rock interface and asperity angle.

The normal stiffness can be determined conveniently from Eq. 3. The relative displacement of the pile–rock interface is calculated by subtracting the current displacement w and maximum displacement w_{st} of the elastic portion (SP1). The maximum displacement is closely related to the rock mass modulus and geological conditions (O'Neill and Hassan 1994). In addition, based on the results of both CNS tests and field load tests, w_{st} lies in the range between 0.5 and 2 mm and the initial slope of f – w relations of rock-socketed drilled shafts decreases as the degree of weathering increases (Seol and Jeong 2007). This range is in general agreement with the observations of Kim et al. (1999). Therefore, w_{st} can be conveniently proposed to be the following linear function of GSI:

$$w_{st} = 2 - 1.5GSI/100 \text{ (mm)}. \tag{7}$$

Fig. 7 Proposed shear load transfer function: **a** shear stress–normal stress curve, **b** shear stress–shear displacement curve



When compared with measured and predicted normal displacement ψ , the elastic deformation of asperity reduces the dilation component and produces a dilation angle less than the initial asperity angle. However, the results of regression analysis using the results of CNS tests and field pile load tests show that the present method is not particularly sensitive to the elastic deformation of asperity at the pile–rock interface. Consequently, the shear transfer function, considering the influential factors of the shaft resistance of rock-socketed drilled shafts, is proposed as the following nonlinear triple curve comprising SP1, SP2, and SP3:

$$f = A\sigma_{ci} \left[\frac{\sigma_{n0} - \left(-\frac{\sigma_{ci}}{m_b} \right)}{\sigma_{ci}} \right]^B \times \frac{w}{w_{st}} \quad (\text{for } w \leq w_{st}) \quad (8a)$$

$$f = A\sigma_{ci} \left[\frac{[\sigma_{n0} + K_n \tan i(w - w_{st})] - \left(-\frac{\sigma_{ci}}{m_b} \right)}{\sigma_{ci}} \right]^B \quad (\text{for } w_{st} < w \leq w_{max}) \quad (8b)$$

$$f = f_{max} \quad (\text{for } w_{max} < w) \quad (8c)$$

where σ_{ci} is the UCS of the weaker materials (rock or pile) and A and B are the strength parameters that depend on the GSI of the rock mass. Strength parameters A and B can be obtained using regression analysis. By normalizing and taking logarithms, Eqs. 8a–8c will be a linear line with slope B and an intercept $\log A$.

Figure 8 shows the variations of peak shear stress τ_{max} against normal stress in the log-transformed coordinates X and Y based on the results of the CNS tests. In Fig. 8, GSI and s were set as 100 and 1, respectively, because test samples are considered to be intact rock, and the value of

m_i was determined directly from rock triaxial compressive tests on the intact rock. Thus, the proposed function suitably represents the peak shear strength of joints, and can properly predict the shear strength of regular sawtooth joints, taking into account their roughness, normal stiffness, and initial normal stress.

The proposed function is validated through field case histories to estimate parameters A and B . To this end, a total of ten large-diameter drilled shafts socketed in rocks with various degrees of weathering are critically analyzed. The test piles under review range from 0.76 to 3.0 m in diameter and 6.4 to 43.8 m in length. Among the ten piles, six tests are examined by the Osterberg cell load testing method. Details of all the tests are given in Table 4: rock type, pile length (L), pile diameter (D), elevation of estimated f – w curve (-E.L), UCS of intact rock (σ_{ci}), rock mass modulus (E_m), rock quality designation (RQD), rock mass rating (RMR), GSI which can be correlated with RMR, roughness angle (i), ultimate unit shaft resistance (f_{max}), material constant for the intact rock (m_i), and initial normal stress (σ_{n0}).

Figure 9 shows the relationship between the strength parameters and GSI. The values of A are constant at about 0.23 and the values of B range from 0.48 to 0.82. Parameter B tends to decrease logarithmically as the GSI of the rock mass increases, and can be approximated, for the sake of simplicity, with a bi-linear curve as follows:

$$B = -0.008 \text{ GSI} + 0.94 \quad (\text{for } \text{GSI} < 45) \quad (9a)$$

$$B = -0.002 \text{ GSI} + 0.67 \quad (\text{for } \text{GSI} \geq 45) \quad (9b)$$

Finally, the proposed shear transfer function of drilled shafts socketed in rocks can be obtained by substituting A and B into Eqs. 8a–8c.

4 Load Transfer Analysis by Coupled Soil Resistance

The load transfer method models discrete elements on the pile and represents the soil as a set of load transfer curves that describe the soil resistance as a function of pile displacements at several discrete points along the pile, including the pile tip. It is implicit that coupled soil resistance in which the response at any point on the interface affects other points is neglected.

The authors proposed a methodology to consider this coupling effect based on a combination of the load transfer method and the elastic method using Mindlin’s equation (Kim et al. 1999). They reported the solution procedure of the methodology to consider the coupling effect, which takes into account the coupled soil resistance. Here, the continuity of the soil mass was considered based on Mindlin’s solution. The vertical displacement at any element due to shear on the other elements is introduced as follows:

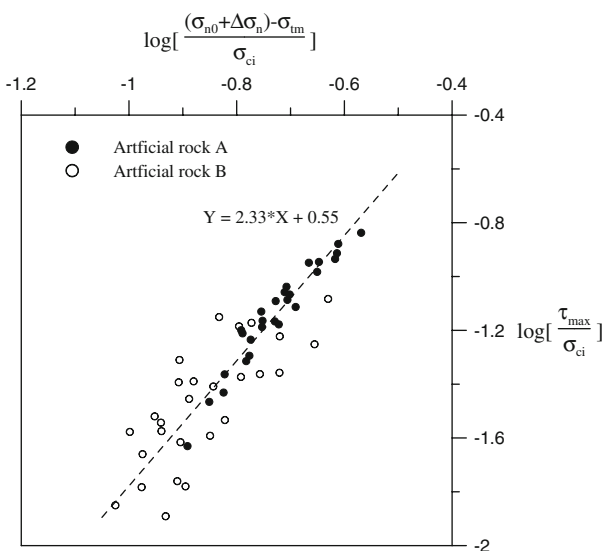


Fig. 8 Result of regression analysis based on CNS test

Table 4 Material properties of test piles

Site	Pile no.	Rock type	<i>L</i> (m)	<i>D</i> (mm)	-E.L (m)	<i>q_u</i> (MPa)	<i>E_m</i> (MPa)	RQD	RMR	GSI ^a	<i>i</i> (°)	<i>f_{max}</i> (kPa)	<i>m_i</i> ^c
Gyeonggi	D2	Gneiss (CW)	13.5	1,000	12.9	48	905	0	22	17	4.6 ^b	>670	33
	D3	Gneiss (CW)	13.5	1,000	12.2	48	974	0	22	17	4.6 ^b	720	33
	D4	Gneiss (HW)	13.5	1,000	12.1	48	1,203	9	31	26	4.6 ^b	>1,100	33
		Gneiss (MW)				48	1,932	40	42	37		1,600	
	D5	Gneiss (MW)	13.5	1,000	12.9	48	2,748	52	45	40	4.6 ^b	1,830	33
Inchon	W8	Granite (MW)	45.1	2,400	44.5	35	2,130	8	–	40 ^e	4.6 ^b	1,400	33
					47.9	35	2,300	–	45 ^e		1,750		
	E7	Granite (MW)	40	2,400	49.0	30	1,480	18	–	35 ^e	4.6 ^b	1,400	33
	E5	Granite (MW)	40.1	3,000	49.5	54	1,630	25	–	45 ^e	4.6 ^b	2,370	33
51.5					54	1,300	–	40 ^e		1,950			
52.5					54	1,300	–	45 ^e		1,630			
Houston	H	Clayshale (SW)	3 ^d	760	9.2	1	70	95	–	95 ^e	4.7	102	9
	D	Clayshale (SW)	5.8 ^d	760	7.0	4	200	82	–	90 ^e	6.2	405	9
	R	Limestone (SW)	4.5 ^d	760	4.0	10	900	88	–	95 ^e	3.7	1,545	10

CW = completely weathered; HW = highly weathered; MW = moderately weathered; SW = slightly weathered

^a GSI = RMR₇₆ = RMR₈₉ – 5 (where, RMR₇₆ > 18, RMR₈₉ > 23)

^b Moderate magnitude of hole roughness angle

^c The value of the Hoek–Brown constant *m* for intact rock (after Hoek and Brown 1997)

^d Length of test socket

^e General reference value presumed without performing field tests

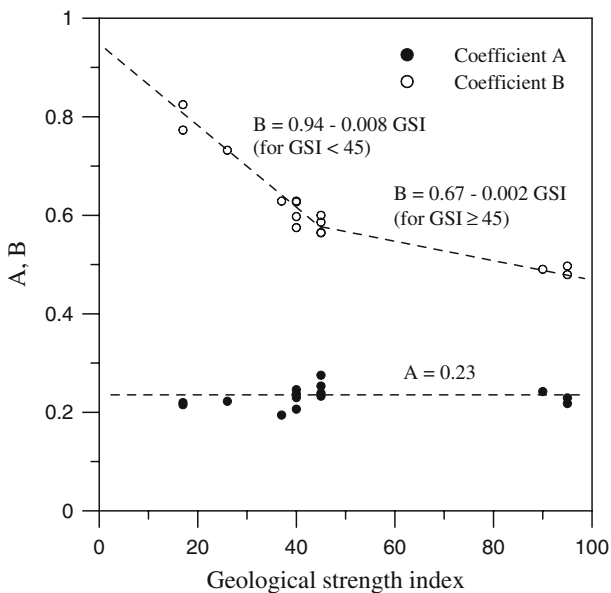


Fig. 9 Strength constants *A* and *B* according to the GSI

$$\{w_s\} = \frac{D}{E_s} [I_s] \{p\} \tag{10}$$

where $\{w_s\}$ is the vertical displacement of soil adjacent to the pile, $\{p\}$ is a pile stress vector, *D* and *E_s* are the pile diameter and Young’s modulus of the soil, respectively,

and $[I_s]$ is the influence factor, which is approximately obtained by integrating Mindlin’s equation to determine the displacement due to a point load within a semi-infinite mass.

As a result of *n* elements and the base, the element of influence factor *I_s* can be classified into two different components: one is *I_{bj}* (*j* = 1 – *n*), which is the toe displacement due to shear stress on an element *j*, and the other is *I_{ij}* (*i* ≠ *j*), which is the vertical displacement factor for *i* due to shear stress on element *j*. Therefore, the pile toe displacement caused by the load transmitted along the pile shaft can be expressed as:

$$w_{bs} = \frac{D}{E_s} \sum_{j=1}^n (I_{bj} f_j) \tag{11}$$

where *f_j* is the shear stress on element *j* and *I_{bj}* is the vertical displacement factor for the base due to shear stress on element *j* (see Fig. 10):

$$I_{bj} = \pi \int_{(j-1)\Delta L}^{j\Delta L} I_p dc \tag{12}$$

where the length of the element ΔL is *L/n*, *c* is the embedded depth to element *j*, and *I_p* is the influence factor for vertical displacement due to a vertical point load (Poulos and Davis 1968; Kim et al. 1999). By substituting

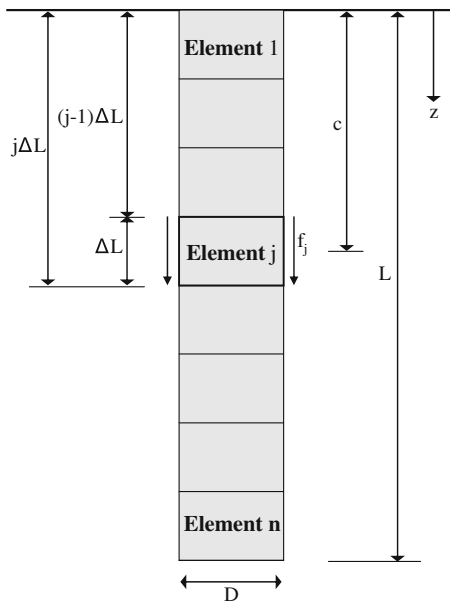


Fig. 10 Geometry of a pile (Poulos and Davis 1968)

Eq. 12 into Eq. 11, the pile toe displacement w_{bs} caused by the load carried by the pile shaft can be calculated.

4.1 Solution Procedure

The mechanical model of a pile under axial loading is shown in Fig. 11. The pile is considered to be composed of a series of deformable springs of length ΔL connected by rigid joints at nodes denoted by the symbol i . The pile stiffness is modeled as a linear spring with stiffness $AE/\Delta L$, where A is the cross-sectional area and E is the modulus of elasticity. External loads Q and support springs S (shaft resistance S_{f-w} of $n + 1$ and toe resistance S_{q-w} of 1) may be placed at each node i . The internal force in each spring is termed the thrust and is denoted by the symbol T . Displacements w are considered positive in the positive x -direction, as shown in Fig. 11. Tensile thrust is considered to be positive. The force–equilibrium equation for any node i can be expressed as follows:

$$-T_i + T_{i+1} + Q_i - S_i(w_i - w_{bs}) = 0 \tag{13}$$

where w_i is the total displacement at node i , w_{bs} is the pile toe displacement caused by the load transmitted along the pile shaft (Eq. 11), so that $w_i - w_{bs}$ represents the relative displacement between the pile and soil. At node 0 (pile head) and node n (pile toe), half-values of the soil reaction stiffness S_{f-w} should be used because the equivalent spring at each node represents the soil reaction stiffness for half of the layer depth, which is equal to half the length of the corresponding element.

From the force–deformation relationships for each spring, the member forces must be:

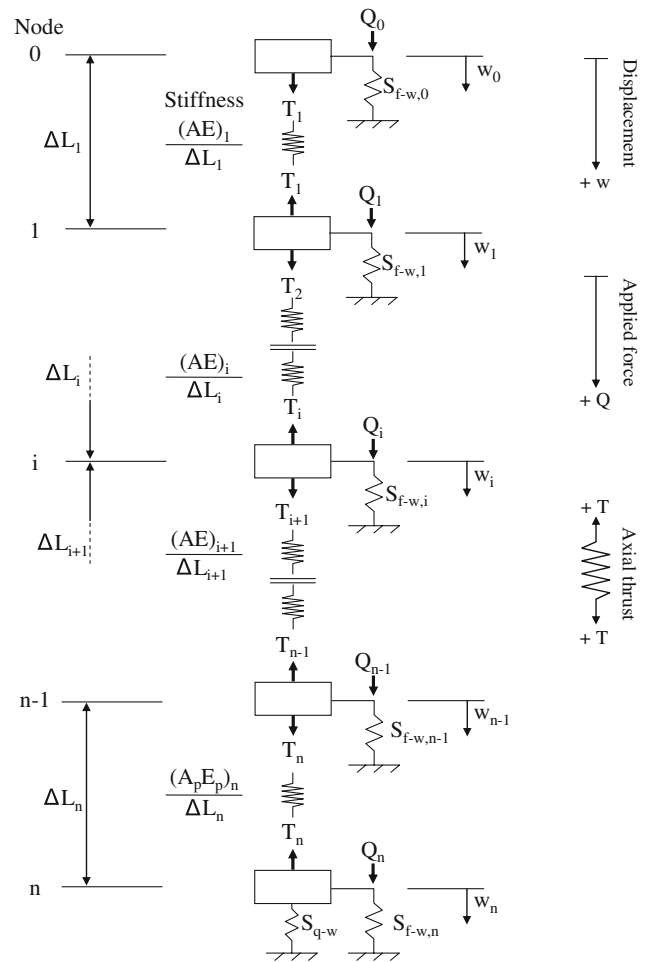


Fig. 11 Mechanical model for an axial beam column

$$T_i = \frac{(AE)_i}{\Delta L} (-w_{i-1} + w_i) \tag{14a}$$

$$T_{i+1} = \frac{(AE)_{i+1}}{\Delta L} (-w_i + w_{i+1}) \tag{14b}$$

A convenient and powerful procedure for solving this problem for nonhomogeneous soil profiles and complicated inelastic transfer functions is to formulate a full set of nonlinear equations by applying Eqs. 13, 14a, and 14b. The nonlinear analyses were performed taking into account the coupled soil resistance effect at the pile–soil interface and were then used in iterative and incremental analysis. The incremental procedure divided the external load into many small and equal increments that were applied sequentially.

5 Validation with Case Histories

The validity of the proposed methodology was tested by comparing the results from the present approach with some of the measured results in detail in the following section.

5.1 Gyeonggi Case

The load transfer characteristics of three instrumented drilled shafts (D2, D4, and D5) reported by Kwon (2004) are compared with the predicted values of the proposed methodology. These piles were founded in completely to moderately weathered gneiss. Figure 12 shows an idealization of the subsurface profile and shaft embeddings for the test piles (D2, D4, and D5). All of the test piles are 1,000 mm in diameter and 13.8 m in length.

Table 5 shows the transfer functions and material properties used in this study: the UCS of an intact rock (σ_{ci}), the soil or rock mass moduli (E_s), the unit weight (γ), the mean roughness angle (i), the geological strength index

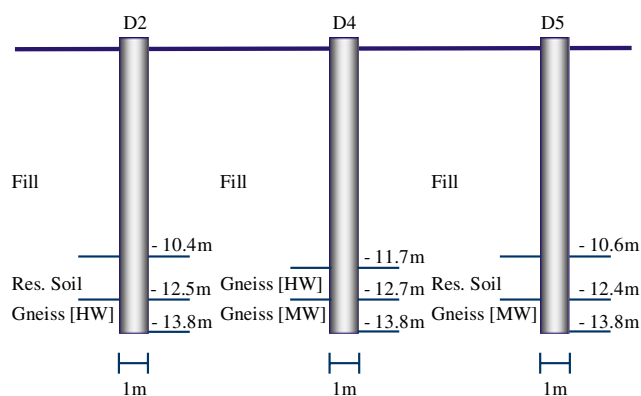


Fig. 12 Subsurface profile and shaft embeddings for test piles (Gyeonggi)

Table 5 Subsurface profile and material properties (Gyeonggi case)

Pile no.	Subsurface profile		Transfer function	Material properties							
	Type	Depth (m)		q_u (MPa)	E_s (MPa)	γ (kN/m ³)	i (°)	GSI	f_{max} (kPa)	w_{max} (m)	
–	Pile	0–13.8	–	33	28,000	23.0	–	–	–	–	
D2	Shaft	Fill	0.3–10.4	Bi-linear	–	–	17.5	–	–	100	0.01
		Residual soil	10.4–12.5	Bi-linear	–	–	18.0	–	–	300	0.01
		Gneiss (CW)	12.5–13.8	Proposed	48	905	21.0	4.6 ^a	17	1,290 ^b	–
	Toe	Gneiss (CW)	–	Hyperbolic ^c	48	905	–	–	–	25,000 ^d	–
D4	Shaft	Fill	0.3–11.7	Bi-linear	–	–	17.5	–	–	100	0.01
		Gneiss (HW)	11.7–12.7	Proposed	48	1,203	21.0	4.6 ^a	26	1,490 ^b	–
		Gneiss (MW)	12.7–13.8	Proposed	48	1,932	21.0	4.6 ^a	37	1,890 ^b	–
	Toe	Gneiss (MW)	–	Hyperbolic ^c	48	1,932	–	–	–	25,000 ^d	–
D5	Shaft	Fill	0.3–10.6	Bi-linear	–	–	17.5	–	–	100	0.01
		Residual soil	10.6–12.5	Bi-linear	–	–	18.0	–	–	300	0.01
		Gneiss (MW)	12.5–13.8	Proposed	48	2,748	21.0	4.6 ^a	40	2,250 ^b	–
	Toe	Gneiss (MW)	–	Hyperbolic ^c	48	2,748	–	–	–	25,000 ^d	–

^a Moderate magnitude of borehole roughness angle

^b Predicted value by $f_{max} = 0.135 P_a (E_m/P_a)^{0.5}$ (Seol and Jeong 2007)

^c Castelli et al. (1992)

^d Ultimate unit toe resistance (q_{max})

(GSI), the ultimate unit shaft resistance (f_{max}), and the critical displacement (w_{max}) of the pile segment which occurs at f_{max} . The properties of the material and interface for the gneiss layer were chosen based on the results of a soil investigation, but those for the fill and residual soil layers were assumed by using general reference values without performing field tests.

The roughness in the f – w model of the gneiss layer is characterized by the chord length and the mean roughness angle, which are then used to generate fractal roughness profiles for the socket wall, as mentioned in the previous section. The borehole roughness for rocks with UCS greater than 20 MPa was represented by a regular sawtooth with a chord length of 50 mm and a roughness angle ranging from 1.1 to 8.0° based on the results of the borehole roughness profiling tests (Table 1). This approach yielded an average roughness angle for the test shafts of 4.6°. Also, the f_{max} used in the interface model of the rock layer was determined by its empirical relationship with the rock mass modulus (Seol and Jeong 2007).

Figure 13 shows the predicted and measured f – w curves for the test piles. The measured shaft resistance did not reach the ultimate state and continued to increase as the displacement increased. This observation agrees with the observation of Williams et al. (1980), who report that the more a rock mass is weathered, the greater the shaft displacement before the ultimate state is reached. As a result, propagation failure occurs gradually. The proposed f – w function generally does a better job of predicting the measured shaft resistance than other load transfer functions

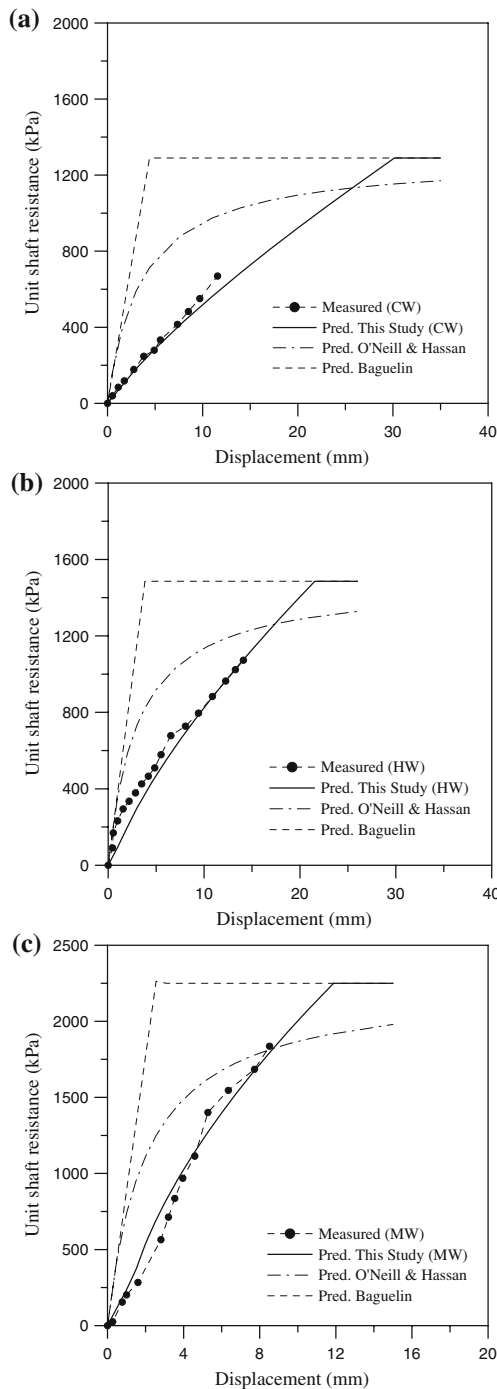


Fig. 13 Shear load transfer function: **a** pile D2, **b** pile D4, **c** pile D5

(Baguelin 1982; O'Neill and Hassan 1994). In particular, the proposed $f-w$ function is in reasonably good agreement with the $f-w$ curves measured by load tests in highly weathered rock.

Figure 14 shows the predicted and observed load settlement curves for the test piles. The proposed methodology (with the proposed $f-w$ function and soil coupling effect) accurately predicts the general trend of the

measured values when compared with the results from the existing method (with only the proposed $f-w$ function). The analysis of all test piles using the existing method has a considerably smaller settlement when compared with the results of the present solution. This clearly demonstrates that, for test piles, there exists soil coupling, which is represented by w_{bs} , so that this set of prediction results

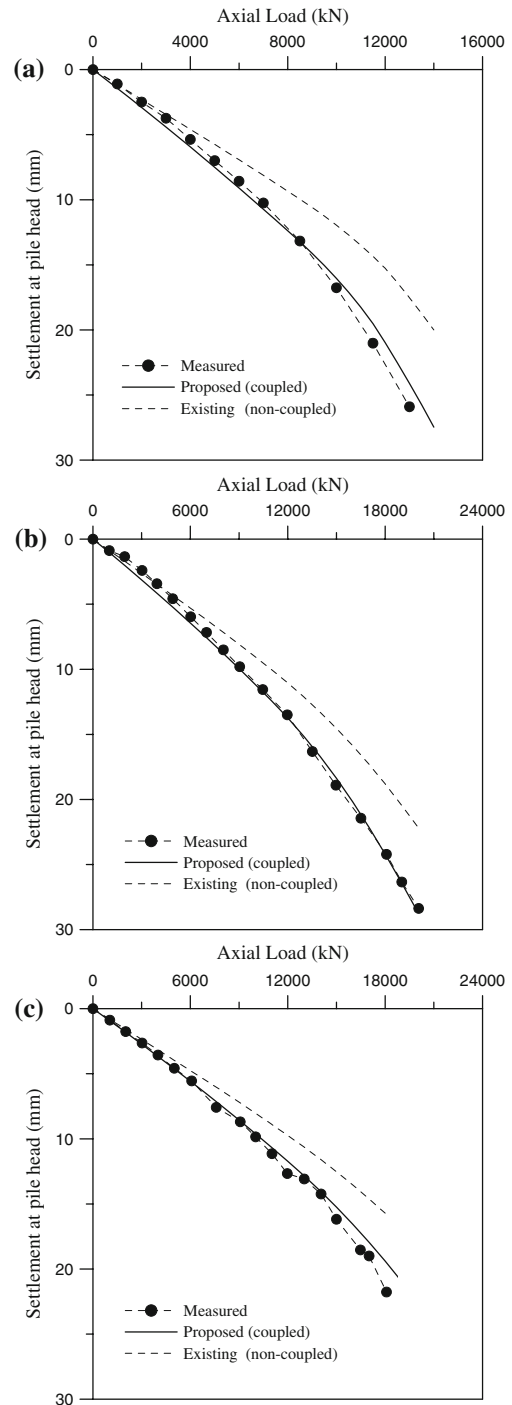


Fig. 14 Load-displacement curves at the pile head: **a** pile D2, **b** pile D4, **c** pile D5

demonstrates the influence of pile–toe settlement due to the transfer of shaft shear loading.

Figure 15 shows the predicted and observed axial load distribution of the test piles. In Fig. 15, only the results of the proposed methodology are presented; results using the existing method are excluded. This is because the force–

equilibrium equations are calculated by excluding w_{bs} , so that the axial load distributions obtained via the present approach are consistent with those of the existing method. It is observed that agreement between the measured and predicted values is generally good.

5.2 Hong Kong Case

The load transfer characteristics of one instrumented drilled shaft installed in volcanic tuff are compared with the predicted values of the proposed load transfer analysis. Figure 16 shows the subsurface profile and shaft embeddings (Zhan and Yin 2000). Test pile V2 is 1,050 mm in diameter and 35.6 m in length. The bitumen coating and cement and bentonite grout on the outside of the test pile were used to minimize the friction developed along the pile shaft, thereby allowing most of the applied load at the pile head to reach the rock socket level. The soil properties and shear transfer functions were chosen to represent the soil and rock based on soil borings and pile load tests. Table 6 shows the transfer function and material properties.

Figures 17 and 18 show a comparison of the load settlement curves and axial load distributions for the test piles, respectively. The proposed methods (with the proposed $f-w$ function and soil coupling effect) accurately predict the general trend of the measured values when the results are compared with the results produced using the existing method (with only the proposed $f-w$ function). Most of the applied load was transferred into the rock socket nearby pile toe due to the bitumen coating and cement bentonite grout; thus, there was a considerable coupling effect caused by the load carried by the pile shaft.

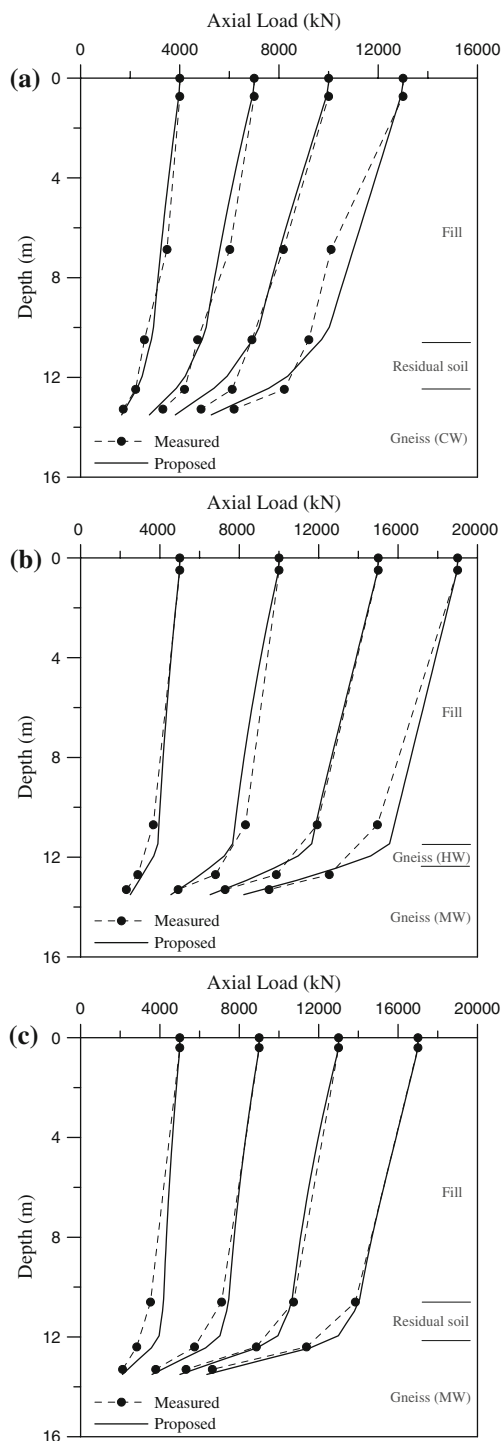


Fig. 15 Axial load distributions: **a** pile D2, **b** pile D4, **c** pile D5

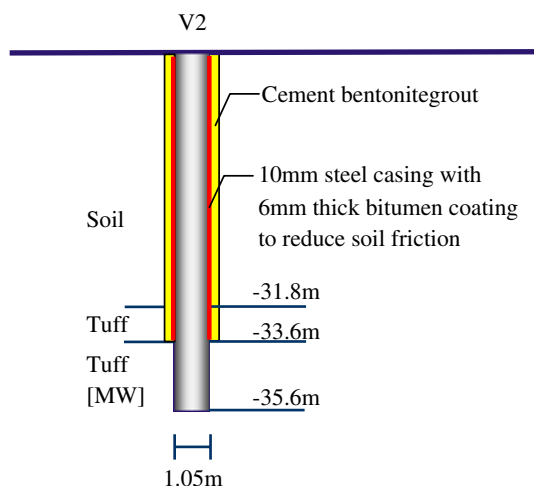


Fig. 16 Subsurface profile and shaft embeddings for the test piles (Hong Kong)

Table 6 Subsurface profile and material properties (Hong Kong case)

Pile no.	Subsurface profile		Transfer function	Material properties						
	Type	Depth (m)		q_u (MPa)	E_s (MPa)	γ (kN/m ³)	i (°)	GSI	f_{max} (kPa)	w_{max} (m)
—	Pile	0–35.6	—	45	41,000	23.0	—	—	—	—
V2	Shaft	Fill	Bi-linear	—	—	17.5	—	—	7	0.01
		Tuff (MW)	Proposed	30	2,000	21.0	4.6 ^a	50	2,700 ^b	—
	Toe	Tuff (MW)	Hyperbolic ^c	30	2,000	—	—	—	25,000 ^d	—

^a Moderate magnitude of borehole roughness angle

^b Predicted value by $f_{max} = 0.135 P_a (E_m/P_a)^{0.5}$ (Seol and Jeong 2007)

^c Castelli et al. (1992)

^d Ultimate unit toe resistance (q_{max})

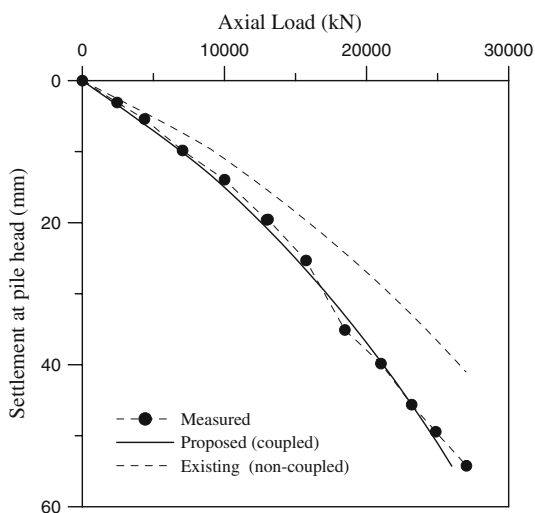


Fig. 17 Load–displacement curves at the pile head (Hong Kong)

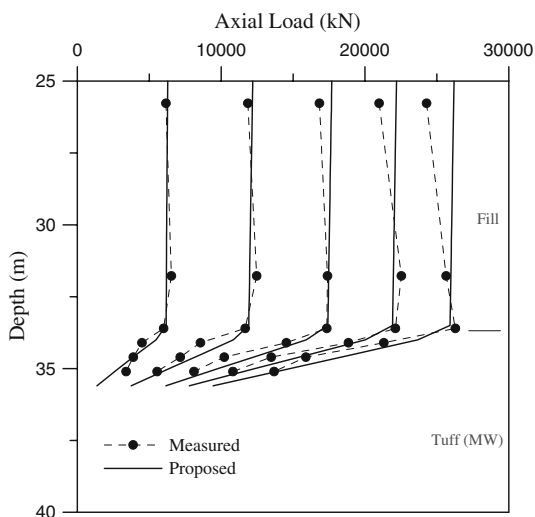


Fig. 18 Axial load distributions (Hong Kong)

6 Conclusions

The main objective of this study is to propose a practical method of rock-socketed drilled shafts that can consider various factors that influence shaft resistance. Through comparisons with case histories, the proposed load transfer function and analytical method are found to be in good agreement with in situ measurements. From the findings of this study, the following conclusions are drawn:

1. Based on the results of constant normal stiffness (CNS) tests, the shear load transfer behavior of rock-socketed drilled shafts can be explained using three sections consisting of an elastic (SP1), elasto-plastic (SP2), and plastic portion (SP3). The shear behavior of the three portions depends largely on the influencing factor of shaft resistance. In addition, the peak shear strength and shear stiffness of SP1 increase as the initial normal stress increases, whereas those of SP2 increase as the roughness angle and normal stiffness increase.
2. By taking into account various shaft resistance factors that are influential under the CNS condition, the new $f-w$ function is appropriate and realistic for representing the shear load transfer characteristics of a drilled shaft socketed in a rock mass. The physical processes modeled theoretically include slippage at the pile–rock interface and frictional–dilative shear behavior.
3. The analysis using the present method with the coupling effect has a considerably larger settlement when compared with the results generated by the existing methods. Soil coupling does exist in the test piles and is represented by w_{bs} .

References

Baguelin F (1982) Rules for the structural design of foundations based on the selfboring pressuremeter test. In: Proceedings of the

- Symposium on the Pressuremeter and its Marine Application, IFP, Paris, France, April 1982, pp 347–362
- Boresi AP (1965) Elasticity in engineering mechanics. Prentice-Hall, Englewood Cliffs
- Carter JP, Kulhawy FH (1988) Analysis and design of drilled shaft foundations socketed into rock. Final report, EL 5918/Project 1493–4/Electric Power Research Institute. Cornell University, Ithaca
- Castelli F, Maugeri M, Motta E (1992) Analisi non lineare del cedimento di un Palo Singolo. *Rivista Italiana di Geotecnica* 26(2):115–135
- Hoek E, Brown ET (1997) Practical estimates of rock mass strength. *Int J Rock Mech Min Sci Geomech Abstr* 34(8):1165–1186
- Indraratna B, Haque A, Aziz N (1998) Laboratory modelling of shear behaviour of soft joints under constant normal stiffness conditions. *Geotech Geol Eng* 16:17–44
- Johnston IW (1994) Movement of foundations on rock. Geotechnical special publication no. 40. Vertical and horizontal deformations of foundations and embankments ASCE, vol 2, pp 1703–1717
- Kim SI, Jeong SS, Cho SH, Park IJ (1999) Shear load transfer characteristics of drilled shafts in weathered rocks. *J Geotech Geoenviron Eng ASCE* 125(11):999–1010
- Kwon OS (2004) Effect of rock mass weathering on resistant behavior of drilled shaft socketed into weathered rock. PhD dissertation, Seoul University
- Lee MH, Cho CH, Yoo HK, Kwon HK (2003) A study on the surface roughness of drilled shaft into rock in Korea. In: Proceedings of the Korean Geotechnical Society Conference, KGS, Seoul, pp 431–438
- Nam MS (2004) Improved design for drilled shafts in rock. PhD dissertation, University of Houston
- O'Neill MW, Hassan KM (1994) Drilled shaft: effects of construction on performance and design criteria. In: Proceedings of the International Conference on the Design and Construction of Deep Foundations, vol 1, Federal Highways Administration, Washington DC, pp 137–187
- Ooi LH (1989) The interface behaviour of socketed piles. PhD dissertation, University of Sydney
- Poulos HG, Davis EH (1968) The settlement behaviour of single axially loaded incompressible piles and piers. *Geotechnique* 18:351–371
- Seidel JP, Collingwood B (2001) A new socket roughness factor for prediction of rock socket shaft resistance. *Can Geotech J* 38(1):138–153
- Seidel JP, Haberfield CM (1995) Towards an understanding of joint roughness. *Rock Mech Rock Eng J* 28(2):69–92
- Seol HI (2007) Load transfer analysis of rock-socketed drilled shafts by considering coupled soil resistance. PhD dissertation, Yonsei University
- Seol HI, Jeong SS (2007) Shaft resistance characteristics of rock-socketed drilled shafts based on pile load tests. *J Korean Geotech Soc* 23(9):51–63
- Taylor WH (1965) Concrete technology and practice, 1st edn. Angus and Robertson, Sydney
- Williams AF, Johnston IW, Donald IB (1980) The design of socketed piles in weak rock. In: Proceedings of the International Conference on Structural Foundations on Rock, Sydney, Australia, May 1980. Balkema, pp 327–347
- Zhan C, Yin J (2000) Field static load tests on drilled shaft founded on or socketed into rock. *Can Geotech J* 37:1283–1294